Toxicology 495 (2023) 153600

Contents lists available at ScienceDirect

Toxicology

journal homepage: www.elsevier.com/locate/toxicol

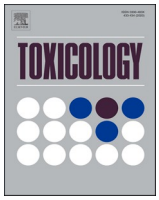

Three-dimensional cultured ampullae from rats as a screening tool for vestibulotoxicity: Proof of concept using styrene

V. Tallandier [a,b], L. Merlen [a], M. Chalansonnet [a,*], S. Boucard [a], A. Thomas [a], T. Venet [a,b], B. Pouyatos [a,b]

[a] French Research and Safety Institute for the Prevention of Occupational Accidents and Diseases (INRS), Toxicology and Biomonitoring Division, Vandoeuvre les Nancy, France

[b] DevAH EA 3450 – Développement, Adaptation et Handicap. Régulations cardio-respiratoires et de la motricité-Université de Lorraine, F-54500 Vandœuvre, France

ARTICLE INFO

Handling Editor Dr. Mathieu Vinken

Keywords:
Three-dimensional culture
Ampulla
Vestibular explants
Endolymph
Potassium
Styrene

ABSTRACT

Numerous ototoxic drugs, such as some antibiotics and chemotherapeutics, are both cochleotoxic and vestibulotoxic (causing hearing loss and vestibular disorders). However, the impact of some industrial cochleotoxic compounds on the vestibular receptor, if any, remains unknown. As *in vivo* studies are long and expensive, there is considerable need for predictive and cost-effective *in vitro* models to test ototoxicity. Here, we present an organotypic model of cultured ampullae harvested from rat neonates. When cultured in a gelatinous matrix, ampulla explants form an enclosed compartment that progressively fills with a high-potassium (K^+) endolymph-like fluid. Morphological analyses confirmed the presence of a number of cell types, sensory epithelium, secretory cells, and canalar cells. Treatments with inhibitors of potassium transporters demonstrated that the potassium homeostasis mechanisms were functional. To assess the potential of this model to reveal the toxic effects of chemicals, explants were exposed for either 2 or 72 h to styrene at a range of concentrations (0.5–1 mM). In the 2-h exposure condition, K^+ concentration was significantly reduced, but ATP levels remained stable, and no histological damage was visible. After 72 h exposure, variations in K^+ concentration were associated with histological damage and decreased ATP levels. This *in vitro* 3D neonatal rat ampulla model therefore represents a reliable and rapid means to assess the toxic properties of industrial compounds on this vestibular tissue, and can be used to investigate the specific underlying mechanisms.

1. Introduction

The cochlear and vestibular labyrinths are sensory structures located in the inner ear. They both rely on sensory hair cells to detect either sound or head movements, respectively. These cochlear and vestibular hair cells are both damaged by the administration of drugs such as aminoglycoside antibiotics (*e.g.* gentamicin) and platinum-based antineoplastic agents (*e.g.* cisplatin), potentially leading to hearing disturbances and vestibular disorders (Steyger, 2021). In the workplace, many industrial compounds are classified as "ototoxic" (Nies, 2012), and the most extensively studied of these are aromatic solvents. Although cochleotoxicity has been demonstrated for many solvents by epidemiological (Johnson, 2007; Sliwinska-Kowalska et al., 2020) and experimental studies (Campo et al., 2001; Gagnaire and Langlais, 2005), no clear *in vivo* data are available on their potential vestibulotoxicity. Nevertheless, it is not unlikely that solvents could target the vestibular receptor *in vivo,* because (1) human and animal studies showed that some aromatic solvents have a negative impact on the vestibular reflexes

Abbreviations: 3D, three-dimensional; ATP, Adenosine triphosphate; *b*-FGF, basic fibroblast growth factors; BrdU, bromodeoxyuridine; CO_2, carbon dioxide; DAPI, 4′,6-diamidino-2-phénylindole; DIV, day *in vitro*; DMEM-F12, Dulbecco's Modified Eagle Medium / Nutrient Mixture F-12; EGF, epithelial growth factor; g_{DR}, delayed rectifier K^+ conductance; H_2O_2, hydrogen peroxide; IGF, insulin-like growth factor; K^+, potassium ion; KCl, potassium chloride; LSD, least-significant difference; MET, mechano-electrical transduction; Myo7a, myosin VIIa; NaCl, sodium chloride; Na/K-ATPase, sodium-potassium adenosine triphosphate; NKCC1, Na-K-Cl co-transporter 1; OHC, outer hair cells; P, postnatal day; PBS, phosphate-buffered saline; rATP, ribonucleotide triphosphates; ROS, reactive oxygen species; SEM, standard error mean; TBST, tris-buffered saline tween; T/SEM, Transmission/Scanning electron microscopy.

* Correspondence to: French Research and Safety Institute for the Prevention of Occupational Accidents and Diseases (INRS), Toxicology and Biomonitoring Division, 1 rue Morvan, F-54519 Vandoeuvre les Nancy, France.

E-mail address: monique.chalansonnet@inrs.fr (M. Chalansonnet).

https://doi.org/10.1016/j.tox.2023.153600
Received 10 June 2023; Received in revised form 24 July 2023; Accepted 26 July 2023
Available online 28 July 2023

(Calabrese et al., 1996; Larsby et al., 1978; Möller et al., 1990; Niklasson et al., 1993; Odkvist et al., 1982; Tham et al., 1982), and (2) we previously demonstrated ionic and histological disruptions in rat utricular explants exposed to these compounds (Tallandier et al., 2021, 2020).

In these previous studies, we used an *in vitro* model initially developed by Bartolami et al. (2011) and Gaboyard et al. (2005), based on an organotypic culture of neonate utricle that develops an endolymphatic compartment. After a few days in culture in a gelatinous matrix, the utricular explants become self-enclosed, and the volume of the lumen progressively increases as it fills with a K^+-rich endolymph-like fluid. The accumulation of K^+ in the endolymphatic compartment is accomplished by Na/K-ATPase and NKCC1 ion-transporters expressed in secretory cells, and MET channels in hair cells (Bartolami et al., 2011; Tallandier et al., 2020). The utricle explant model can be used to assess both the functional and morphological consequences of exposure to aromatic solvents by recording variations in the endolymphatic K^+ concentration, and performing histological analyses. Our results suggested that this model can rapidly and reliably discriminate the vestibulotoxicity potency of industrial compounds (Tallandier et al., 2021). Despite this success, there was a clear need to expand this model to another vestibular tissue that had not previously been investigated, the *crista ampullaris*. The use of explants from neonate rat ampullae would make the model more ethical – as each animal could provide up to six similar samples – and more informative about the effects of industrial compounds on this portion of the vestibular receptor.

The study presented here was designed to respond to the following objectives: 1) to develop a 3D cultured crista ampullaris model that regenerates an endolymphatic compartment filled with a high-K^+ fluid; 2) to use this *in vitro* system to evaluate the vestibulotoxic effects of styrene.

Inhibitors of K^+ efflux and influx were used to assess the resulting effects of their inhibition on endolymphatic K^+ concentration. Morphological features of the different cell types composing the 3D ampullae were observed thanks to histological analyses. As intracellular energy levels and mitochondrial function are rapidly compromised in necrosis and not in apoptosis, ATP levels in our model were quantified to determine cell death fate (Tsujimoto, 1997). The model was then used to assess the adverse effect of styrene, a widely-used aromatic solvent with known cochleotoxic properties (Campo et al., 2001; Fetoni et al., 2021, 2016; Sliwinska-Kowalska et al., 2020) and deleterious effects on the sensory-motor integration of vestibular pathways (Calabrese et al., 1996; Gans et al., 2019; Larsby et al., 1978; Möller et al., 1990; Niklasson et al., 1993; Odkvist et al., 1982; Tham et al., 1982; Zamyslowska-Szmytke and Sliwinska-Kowalska, 2011) which has a demonstrated toxic effect on utricular explants (Tallandier et al., 2020).

2. Materials and methods

2.1. Animals

Pregnant female Long-Evans rats were supplied by Janvier Laboratories (Le Genest-St Isle, France) and housed individually in cages (surface: 1032 cm^2; height: 20 cm) from their arrival (15th day of pregnancy) until they gave birth. Temperature and relative humidity were maintained at 22 ± 2 °C and 55 ± 15%, respectively, with a 12-h light:12-h dark cycle. Food and water were available *ad libitum*. Birth was natural, and newborns were used within four days of birth (P0-P4). All experiments were performed according to the Guide for Care and Use of Laboratory Animals promulgated by the European parliament and council (European directive 2010/63/EU, 22 September 2010), and the animal facility where the rats were housed is fully accredited by the French Ministry of Agriculture (Authorization N° D 54–547–10).

2.2. Three-dimensional culture of crista ampullaris explants

Newborn rats (P0-P4) were decapitated, and temporal bones were placed in Leibovitz's L-15 medium. Ampullae were aseptically removed and care was taken to preserve the epithelium covering the ampullar crest. The *crista ampullaris* were stripped from the semi-circular duct to retain only the ampullae. Explants were then placed on 10 µL of Matrigel® (Corning, NY, USA) on 12-mm diameter laminin-coated (10 µg/mL) glass coverslips (Sigma-Aldrich, Saint-Louis, MO, U.S.A.). Structures were positioned so that the base of the sensory epithelium faced the coverslip. To solidify the matrix, samples were incubated at 37 °C for 30 min in a 95% O_2 / 5% CO_2 atmosphere at saturating humidity. Embedded explants were then covered with Dulbecco's Modified Eagle Medium / Nutrient Mixture F-12 (DMEM-F12, Thermo Fisher Scientific, Waltham, MA, USA) supplemented with 2% N-2 (Life Technologies, Carlsbad, California). Cultured ampullae were maintained at 37 °C under a humidified 5% CO_2 atmosphere, renewing half of the culture medium three times per week. After incubation for 24 h, explants sealed themselves to delimit a compartment filled with an endolymph-like fluid. The day of seeding was considered as 0 day *in vitro* (DIV).

2.3. Recording K^+ concentration

Ion-sensitive microelectrodes were used to determine the K^+ concentration in the endolymphatic compartment of 3D ampullar explants. Borosilicate glass capillaries with filament (1B100F-4; WPI, Sarasota, FL, USA) were melted and pulled using a vertical electrode puller (PUL-100 Microprocessor-controlled micropipette puller, WPI, Sarasota, FL, USA) before baking for 2 h at 200 °C. The inside of the microelectrode was silanized with dichlorodimethylsilane (Sigma-Aldrich, Saint-Quentin Fallavier, France) vapor (5 min at 100 °C). Microelectrodes were then baked once again for 4 h at 200 °C to eliminate all traces of moisture. The microelectrode tip was backfilled with a membrane liquid K^+ ion exchanger (Potassium Ionophore I – Cocktail B, Sigma-Aldrich, Saint-Quentin Fallavier, France) before filling the barrel with 150 mM KCl. The microelectrode was used only if its impedance was comprised between 70 and 200 MΩ. Selected microelectrodes were then connected to the input of a differential electrometer amplifier (HiZ-223 Warner Instruments, Hamden, USA). The reference electrode was immersed in calibrating solutions or culture medium to close the electrical circuit. A 3160-A-022 analyzer (Brüel & Kjær, Nærum, Denmark) was connected to the amplifier output to monitor the electrical signal. Acquisition was automated using Pulse® software (LabView). The electrical signal from the microelectrode was calibrated against a decreasing range of KCl concentrations (150, 100, 75, 50, 20 and 10 mM) before measuring K^+ in the endolymphatic compartment. Calibration solutions contained the appropriate amount of NaCl to maintain a final cation concentration of 150 mM. The Nernst slope of ion-sensitive microelectrodes was 57.6 ± 3.9 mV / decade [K^+] (n = 50).

To record the K^+ concentration in the endolymphatic compartment, the ampullar explant was placed on the microscope stage and immersed in culture medium. The microelectrode was slowly inserted into the endolymphatic compartment under the light microscope. The electrical signal took a few seconds to stabilize and once stabilized, the electrical potential was recorded. Deflated explants during the initial four DIV were excluded from the study.

2.4. BrdU staining

Bromodeoxyuridine (BrdU) staining was used to track cell division during culture development. Samples were incubated with 100 µM BrdU from 0 DIV up to 2 DIV. Images of BrdU-positive cells were obtained by immunohistology on 4-µm sections of cultured explants. (see §2.9).

2.5. Pharmacological treatment

To investigate K^+ efflux and influx mechanisms in 3D cultured ampullae, samples were incubated with molecules known to perturb transmembrane K^+ transport – ouabain, which inhibits Na/K-ATPase

activity; bumetanide, which inhibits NKCC1 (Marcus et al., 1994); and gadolinium, which perturbs MET channel activity (Kimitsuki et al., 1996). The three inhibitors were purchased from Sigma-Aldrich (Saint-Quentin Fallavier, France). At 7 DIV, explants were exposed to ouabain (0.15, 0.5 or 1 mM) for 2 h, bumetanide (0.05, 0.1 or 0.15 mM) for 30 min, or gadolinium (0.1, 0.3 or 1 mM) for 2 h. The effect of each inhibitor was determined by measuring the endolymphatic K^+ concentration. In parallel, control cultures were incubated in the same conditions with the corresponding vehicle (NaCl 0.9% or ultrapure water).

2.6. Styrene exposure

Styrene (99.9%, Acros Organics, Illkirch, France) was mixed with DMEM-F12 medium (Thermo Fisher Scientific, Waltham, MA, USA) in a volumetric flask to prepare working solutions (0.5, 0.75 and 1 mM). Then, the styrene-enriched culture medium and N-2 (2%, v / v) were transferred into 8-mL glass headspace vials, in which the explants were placed. Vials were completely filled and sealed with a Teflon-faced butyl rubber septum and an aluminum crimp cap to avoid solvent evaporation. Cultures were maintained in these conditions between 2 and 72 h before measuring K^+ concentration or ATP levels at 7 DIV. Control cultures were placed in sealed vials filled with solvent-free medium for the same period.

2.7. Preparation of tissue sections for light and transmission electron microscopy

Cultured explants were fixed with 2.5% glutaraldehyde in 0.2 M cacodylate buffer for 24 h. Samples were rinsed in 0.2 M cacodylate buffer and post-fixed for 1 h with 1% osmium tetroxide in the dark. Then, ampullae were dehydrated in graded ethanol concentrations up to 100% and soaked in resin / propylene oxide solutions, 50/50% followed by 75/25%, before embedding them in pure epoxy resin. The resin was polymerized for 24 h at 60 °C. Transversal sections for light and transmission electron microscopy were cut with a Leica UC7 ultramicrotome. Semi-thin Section (2.5 μm) were stained with toluidine blue (Sigma-Aldrich, Saint-Quentin Fallavier, France) and observed with an optical microscope (BX41, Olympus, Tokyo, Japan). Ultra-thin sections (0.08 μm) were stained with uranyl acetate and lead citrate, and observed with a transmission electron microscope (HT 7700, Hitachi).

2.8. Scanning electron microscopy

Ampullae were fixed with 2.5% glutaraldehyde in 0.2 M cacodylate buffer for one day. Then, the epithelium covering the ampullar crest and cupula were gently peeled away from the surface under a binocular microscope. After rinsing in 0.2 M cacodylate buffer, samples were post-fixed with 1% osmium tetroxide for 1 h in the dark, and rinsed once again. After dehydration in graded ethanol solutions up to 100%, samples were dried in a critical-point dryer using liquid CO_2 (EM CDP300, Leica). Dried samples were then sputter-coated with gold and observed with a scanning electron microscope (7400 F, JEOL).

2.9. Immunostaining

Cultured Ampullae were fixed with 4% buffered-formaldehyde (pH 6.9) for 24 h. After rinsing with phosphate-buffered saline (PBS), samples were dehydrated in graded ethanol solutions up to 100%. After clearing in xylene, vestibular structures were embedded in paraffin. Embedded ampullae were then cut into 4-μm transversal sections with a microtome (HM 34OE, Microm). Sections were dewaxed in xylene and rehydrated in ethanol, using solutions with decreasing concentrations. Heat-induced antigen retrieval was performed at 120 °C for 5 min in sodium citrate buffer (10 mM, pH 6). Sections were rinsed with Tris-Buffered Saline Tween (TBST), endogenous peroxidase activity was blocked with 3% H_2O_2 for 5 min, and nonspecific antibody binding sites were blocked for 1 h with a solution containing normal serum at room temperature. Sections were then incubated overnight at 4 °C with primary antibodies diluted in their corresponding blocking solutions: anti-Na/K-ATPase α-1 monoclonal mouse antibody (dilution 1/1000, Merck Millipore, MA, USA, 05–369), anti-BrdU monoclonal mouse antibody (dilution 1/200, Cell Signaling, MA, USA, 5292 S), and anti-Myo7a polyclonal antibody (dilution 1/200, Proteus Bioscience inc., CA, USA, 25–6790). The next day, samples were rinsed with TBST-1X.

Anti-Na/K-ATPase and anti-BrdU binding were enzymatically detected. Sections were incubated for 30 min at room temperature with the appropriate detection reagent: peroxidase enzyme (SignalStain® Boost Detection Reagent, Cell Signaling) for Na/K-ATPase detection, or alkaline phosphatase enzyme (ImmPRESS®-AP Horse Anti-Mouse IgG Polymer Detection kit, Vector Laboratories, Premanon, France) for BrdU detection. The immunostaining was revealed with 3,3′-diaminobenzidine (DAB) for Na/K-ATPase staining and with ImmPACT Vector Red AP Substrate Kit (Vector Laboratories, Premanon, France) for BrdU staining. Sections were counterstained with Mayer Haemalum before mounting for observation under an optical microscope (BX41, Olympus, Tokyo, Japan).

Myosin VIIa (Myo7a) was detected by immunofluorescence on sections incubated for 1 h at room temperature in the dark with secondary antibody (Alexa 488-conjugated donkey anti-rabbit IgG diluted in normal donkey serum; dilution 1/200, Thermo Fisher Scientific, Waltham, MA, USA). After rinsing in TBST-1X, sections were mounted in Prolong™ Gold antifade mounting medium with 4′,6-diamidino-2-phenylindole (DAPI) (Invitrogen, Thermo Fisher Scientific, Waltham, MA, USA). Fluorescent images were acquired on an AxioScan.Z.1 slide scanner (Zeiss, Marly-le-Roi, France).

2.10. Measuring ATP levels

Total ATP levels in cultured ampullae were quantified using the Cell Titer-Glo® 3D Cell Viability Assay (Promega, Charbonnières-les-Bains, France). Cellular lysis of the samples and the bioluminescence reaction were performed according to the manufacturer's protocol. Briefly, samples were harvested in 100 μL of Cell Titer-Glo® 3D reagent and incubated for 30 min. A standard curve produced with (Ribonucleotide triphosphates; Promega, Charbonnières-les-Bains, France) was used to determine ATP concentrations Luminescence was measured using a Synergy™ HTX Multi-Mode microplate reader (BioTek instruments, Colmar, France). Results were normalized relative to control values.

2.11. Statistical analysis

Data were expressed as mean ± standard error of the mean (SEM). A one-way ANOVA was used to analyze differences between experimental and control groups. Statistical results were expressed as follows: F(dfb, dfr) = F-ratio; p = p value, where dfb is the number of degrees of freedom between groups, and dfr is the number of residual degrees of freedom. The statistical significance threshold was set at $p = 0.05$. A post-hoc least-significant difference (LSD) test was run to compare variations between "DIV" groups, and Dunnett's post-hoc tests were applied to compare variations in K^+ concentrations and ATP levels between control and treated groups.

3. Results

3.1. 3D ampullar explants develop an endolymphatic compartment

Fig. 1 A displays the growth of an ampulla isolated from a newborn rat at P2. A small vesicle first appeared at 1 DIV and swelled until 5 DIV. Its volume stabilized thereafter.

To observe cell proliferation during culture development, we used BrdU staining (Fig. 1B). BrdU was added to culture medium on the day of seeding in gelatinous matrix, and incorporation was measured 48 h

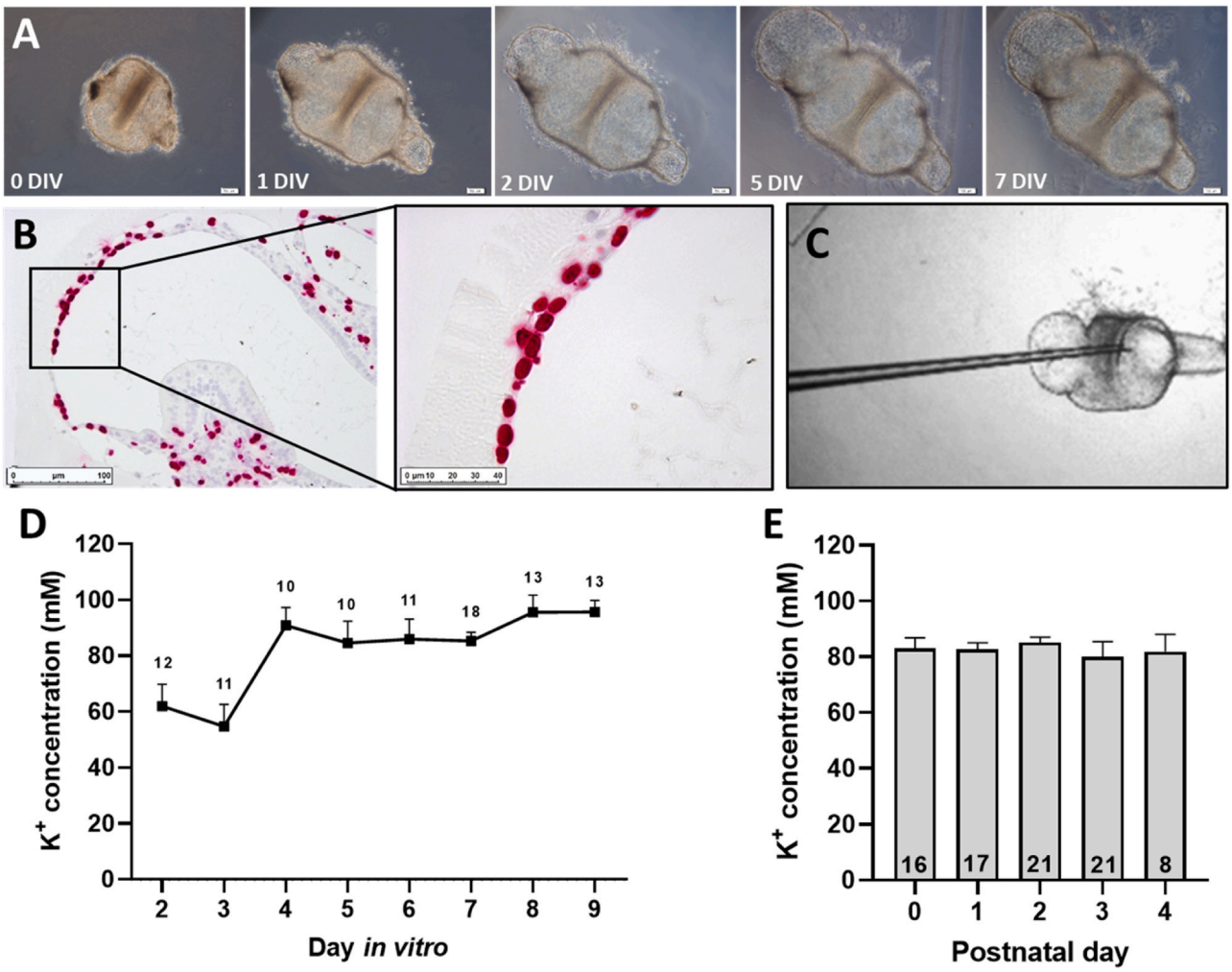

Fig. 1. Development of 3D cultured ampullar explants. (A) Newborn rat ampullae harvested at postnatal day 2 (P2) were observed by light microscopy from 0 to 7 days *in vitro* (DIV). Scale bar = 100 μm. (B) BrdU immunostaining (red) performed in 2-DIV ampullae (P1). BrdU was added to culture media at 0 DIV, after 48 h (2 DIV) samples were fixed. The higher magnification area is delineated by a black square in **B**. (C) Photograph of a cultured ampulla taken during measurement of K^+ concentration using a K^+-ion-sensitive microelectrode. (D) Endolymphatic K^+ concentration measured from 2 DIV to 9 DIV (P0-P4). (E) Endolymphatic K^+ concentrations of 7-DIV cultured ampullae obtained from newborn rats at ages ranging from P0 to P4. Data are expressed as mean ± SEM. Number of samples are indicated above each symbol (D) or in each histogram bar (E).

later. BrdU immunostaining at 2 DIV was localized in the nuclei of the supporting cells covering the *crista ampullaris*, *i.e.* the canalar cells. This pattern indicates that these cells proliferated during the first two days of culture.

The K^+ concentration in endolymph-like fluid was measured between the 2nd and 9th DIV using an ion-sensitive microelectrode (Fig. 1C). K^+ levels increased rapidly from 3 DIV to 4 DIV (54.7 ± 7.9 mM at 3 DIV to 90.8 ± 6.4 mM at 4 DIV), reaching a plateau thereafter (Fig. 1D). One-way ANOVA revealed a difference in K^+ concentration as a function of the DIV [$F = (7, 90) = 5.93$; $p < 0.001$]. Post-hoc comparisons between groups indicated that K^+ concentrations at 2 DIV and 3 DIV were significantly lower than those measured between 4 DIV and 9 DIV ($p < 0.05$). The endolymphatic K^+ concentration was also measured in 7-DIV explants derived from newborn rat ampullae harvested at different postnatal days (Fig. 1E). Age at the time of harvest had no significant effect [$F (4, 82) = 0.25$; $p = 0.905$] on the K^+ concentration at 7 DIV.

3.2. Cellular organization of 3D cultured ampullae

The high potassium concentration of the endolymphatic compartment of the cultured ampullae (Fig. 2A) is maintained by different types of epithelial cells, which balance K^+ secretion and absorption. Fig. 2B displays a semi-thin section of a 7-DIV cultured ampulla showing a clearly-delimited boundary between endolymph and extracellular medium. The sensory epithelium (*crista ampullaris*) was composed of hair cells (HC) and intercalated supporting cells (SC) (Fig. 2B and C). A monolayer of secretory cells bordering each side of the *crista ampullaris* was identifiable. Secretory areas were composed of transitional cells (TC) in direct contact with the sensory epithelium and cuboidal dark cells (DC) (Fig. 2B and D). The remainder of the epithelium was composed of elongated canalar cells (CaC), which allowed the cultured ampulla to seal itself, creating the barrier between the endolymphatic space and the culture medium (Fig. 2B and E).

Semi-thin sections of 7-DIV 3D cultured ampullae revealed a saddle-shaped sensory epithelium. In some cases, the cupula was not fully removed during dissection. Then, the remaining part of the cupula, embedding the stereociliae of the hair cells, could be distinguished at the apical level of *crista ampullaris*. Immunostaining for Myo7a indicated that hair cells were distributed along the *crista ampullaris* (Fig. 3A and B). The sensory epithelial surface of a 7-DIV ampullar explant was analyzed by SEM (Fig. 3C-E). The *crista ampullaris* appeared thin and curved, and numerous hair bundles were evenly distributed all over its surface (Fig. 3C and D). Each ciliary bundle was encircled by microvilli

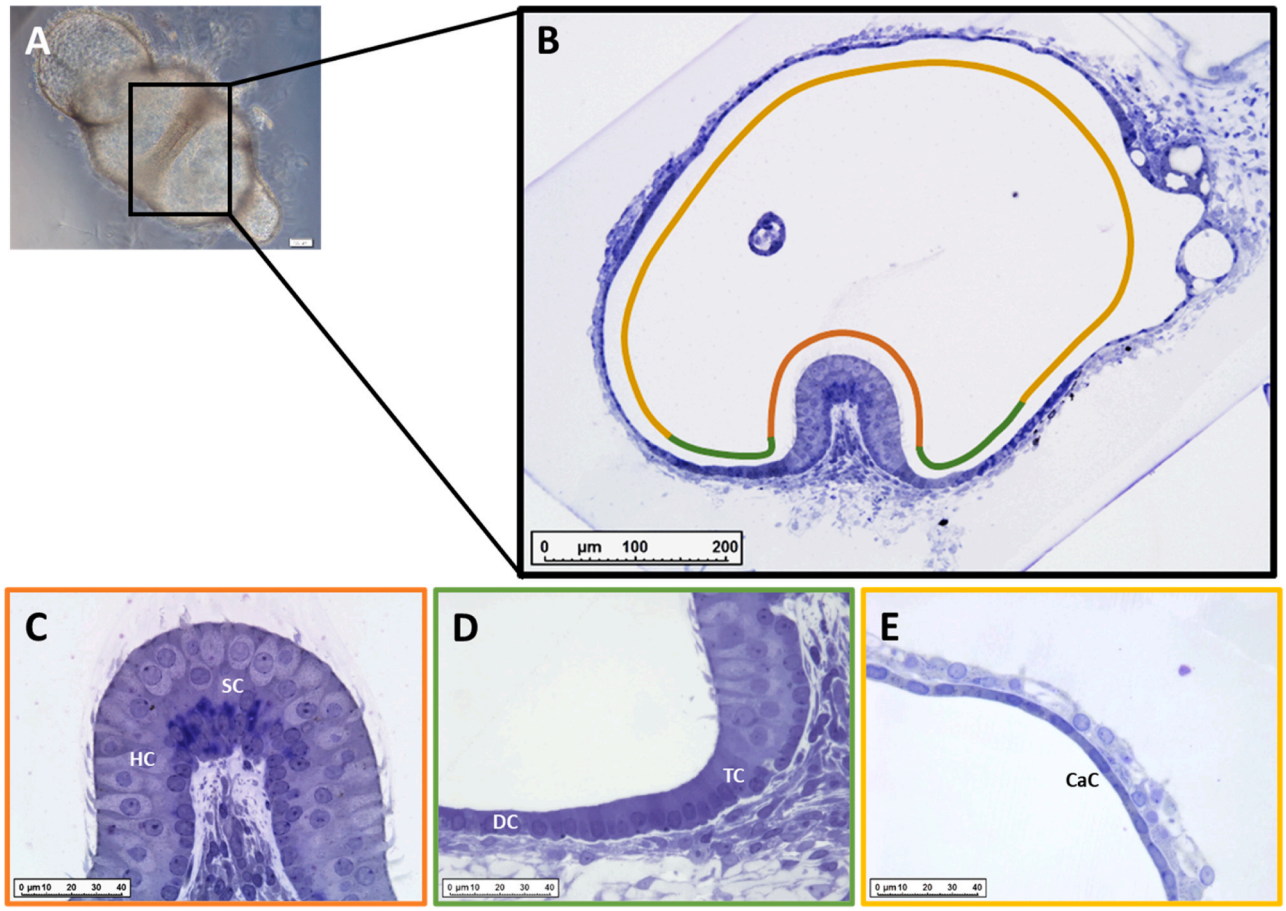

Fig. 2. Cellular organization of 7-DIV 3D cultured ampullae. (A) Ampulla cultured in a 3D matrix for 7 days. Scale bar = 100 µm (B) Transverse semi-thin sections of 7-DIV cultured ampullae obtained from P1 newborn rat observed under light microscopy. The sensory epithelium is indicated in orange, secretory areas in green, and the canalar cell area in yellow. (C) The sensory epithelium is composed of hair cells (HC) interspersed between supporting cells (SC). (D) The secretory areas are composed of elongated transitional cells (TC) and cuboidal dark cells (DC). (E) Canalar cells (CaC) constitute the remainder of the epithelium; they allow the cultured explant to seal itself.

expressed on the apical side of supporting cells. A kinocilium, distinguishable by its longer size, was observed next to the stereocilia. Two types of hair bundles could be distinguished by their length (Fig. 3E): "tall" hair bundles (white arrow) and "short" ones (black arrow). Dechesne et al. (1986) showed that the size of hair bundles continued to increase during the first postnatal week in rats and suggested that short hair bundles were immature while long ones could be considered as mature.

The ultrastructure of the sensory epithelium of 3D cultured ampullae was observed by transmission electron microscopy (TEM) at 7 DIV (Fig. 3F-H). Sensory hair cells could be distinguished from supporting cells by their less electron-dense cytoplasm and their apical hair bundle (Fig. 3G-H). Supporting cells had microvilli on their apical side and their nucleus was located in basal position (Fig. 3F). Two types of hair cells were distinguished according to their morphology: pyriform type I hair cells, and columnar type II hair cells. Transitional cells alongside hair cells delimited the sensory epithelium (Fig. 3F).

The gross morphology of the secretory area was observed on transverse semi-thin sections of 3D cultured ampullae (P1) at 7 DIV (Fig. 4A). Immunostaining for Na/K-ATPase revealed strong expression of this ion pump on the basolateral side of dark cells (Fig. 4B and C). Transitional cells were present between the sensory epithelium and the dark cell area on either side of the crista. Ultrastructural analyses by TEM revealed the morphological features of transitional and dark cells (P1; J7) (Fig. 4D-F). Transitional cells had a clearer cytoplasm than dark cells, and an elongated shape. These cells possessed apical microvilli and a basal nucleus (Fig. 4.D and E). Dark cells were identified based on their cuboidal shape and the large number of vacuoles present in supranuclear and infranuclear regions. Unlike transitional cells, dark cells had no microvilli on their apical side, but they did display cytoplasmic invaginations extending toward the basal side of the membrane, and an irregular nucleus (Fig. 4E and F). Taken together, these histological observations indicated that all vestibular cell types were well-preserved in explants cultured for 7 DIV in the gelatinous matrix and had morphological characteristics similar to *in vivo* ampullae.

3.3. *Effects of inhibitors on endolymphatic K^+ concentration*

The Na/K-ATPase ion pump (Fig. 4B-C) and the co-transporter NKCC1 expressed at the basolateral side of secretory cells both secrete K^+ into the endolymphatic compartment. Conversely, the mechano-electrical transduction (MET) channels expressed in hair-cell stereocilia are involved in transferring K^+ ions from the endolymph to the perilymph. Inhibition of Na/K-ATPase by ouabain (0.15, 0.5 or 1 mM for 2 h), NKCC1 by bumetanide (0.05, 0.1 or 0.15 mM for 30 min), and MET channels by gadolinium (0.1, 0.3 and 1 mM for 2 h) was used to evaluate their effect on endolymphatic K^+ concentration in 7-DIV ampullar explants (Fig. 5).

Treatment with ouabain and bumetanide significantly decreased the K^+ concentration in the endolymphatic compartment [ouabain: $F(3, 28) = 11.16$; $p < 0.001$ – bumetanide: $F(3, 39) = 3.88$; $p = 0.016$]. The 2-h treatment with ouabain caused a dose-dependent decrease in K^+

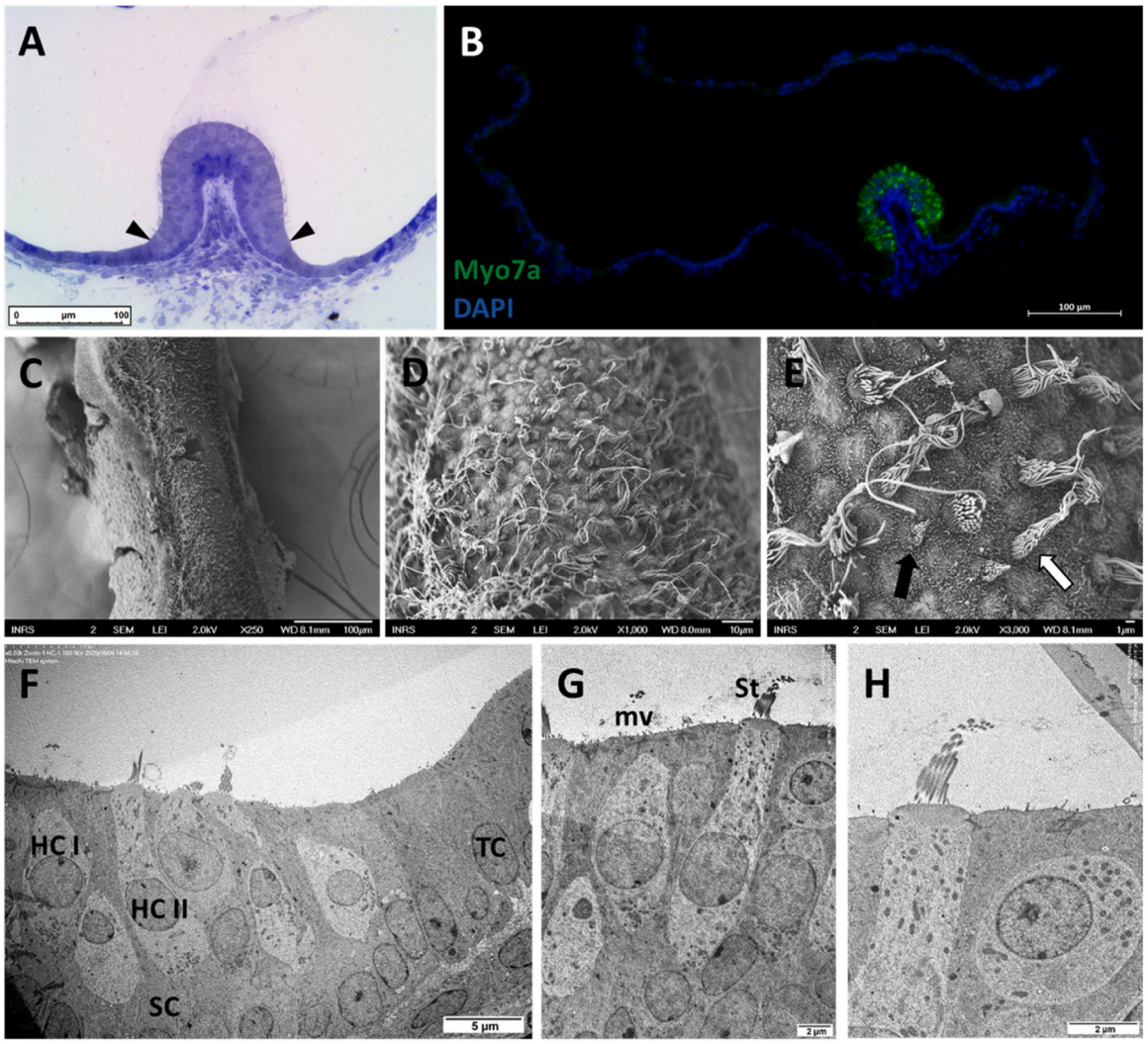

Fig. 3. Sensory epithelium of 7-DIV cultured ampullae. (A) Semi-thin section of 3D cultured ampullae obtained from P1 newborn rats observed under light microscopy. The sensory epithelium is delimited by the two black arrowheads. (B) 3D cultured ampullae (P1) labeled with antibodies directed against Myo7a (green) observed under fluorescence microscopy. Cell nuclei were stained with DAPI (blue). (C-E) Apical surface of the ampullar crest of a 3D explant (P3) observed by scanning electron microscopy. (C) Curved ampullar crest. (D) Zoom on the central part of the *crista ampullaris*. Stereociliary bundles are distributed along the crista. (E) The hair cell displays oriented stereociliae topped by a kinocilium (white arrow) and immature hair bundles (black arrow). Supporting cells are interspersed between hair cells and had numerous microvilli. (F-H) Ultrastructure of the sensory epithelium of cultured ampullae (P1; J7), as observed using transmission electron microscopy. The sensory epithelium is composed of supporting cells (SC) expressing microvilli (mv) on their apical side. Two types of hair cells express stereocilia (St): pyriform type I hair cells (HC I) and columnar type II hair cells (HC II). Transitional cells (TC) are in direct contact with the sensory epithelium.

concentration, that was already significant ($p = 0.041$) at the lowest tested dose (0.15 mM). Treatments with 0.15, 0.5 and 1 mM ouabain decreased K^+ concentration by 24% (66.7 ± 7.4 mM), 41% (51.6 ± 6.9 mM; $p = 0.001$) and 60% (34.3 ± 7.0 mM; $p < 0.001$), respectively, compared to vehicle (87.9 ± 3.8 mM).

Treatment with bumetanide also decreased the K^+ concentration, but to a more modest extent. Only the highest dose (0.15 mM) caused a significant ($p = 0.008$) decrease (bumetanide: 55.1 ± 10.7 mM *versus* control: 87.6 ± 4.5 mM; −37%).

In contrast, treatment with gadolinium for 2 h increased the K^+ concentration [$F(3, 56) = 2.618$; $p = 0.059$]. Significance was reached only with the highest dose (1 mM), which led to a 25% (102.2 ± 3.1 mM; $p = 0.028$) increase in concentration compared to the control group (81.4 ± 4.9 mM).

3.4. Effects of styrene exposure

To evaluate effect of styrene on the endolymphatic K^+ concentration, cultured ampullae (P0–4, J7) were exposed to styrene (concentrations: 0.5, 0.75, and 1 mM) for 2 h or 72 h (Fig. 6). To avoid any interaction between the effect of styrene and culture development, samples were exposed from the 4th to the 7th DIV for the 72-h exposure condition, when the K^+ concentration is the most stable (Fig. 1).

Fig. 6 shows that exposure to styrene for 2 or 72 h caused the endolymphatic K^+ concentration to decrease [2-h exposure: $F(3, 54) = 5.364$; $p = 0.002$ – 72-h exposure: $F(3, 49) = 18.78$; $p < 0.001$]. Exposure to styrene for 2 h significantly decreased the K^+ concentration – by 24% with 0.75 mM (64.2 ± 4.3 mM; $p = 0.011$) and by 27% with 1 mM (61.0 ± 6.4 mM; $p = 0.005$) – compared to the control group (84.5 ± 2.7 mM). No effect was seen with 0.5 mM styrene. Although effects with the two lowest doses were not significant when cultures were treated for a longer duration (72 h), treatment with 1 mM styrene led to a drastic decrease (−70%) in K^+ concentration (25.8 ± 7.6 mM *versus* 86.6 ± 6.8 mM in controls, $p < 0.001$).

Fig. 7 displays light microscopy images of epithelial cells in cultured ampullae (P0–4, 7DIV) exposed to styrene for 2 or 72 h and in control samples. The sensory epithelium of control samples displayed healthy-looking hair cells with ciliary bundles at their apical surface and

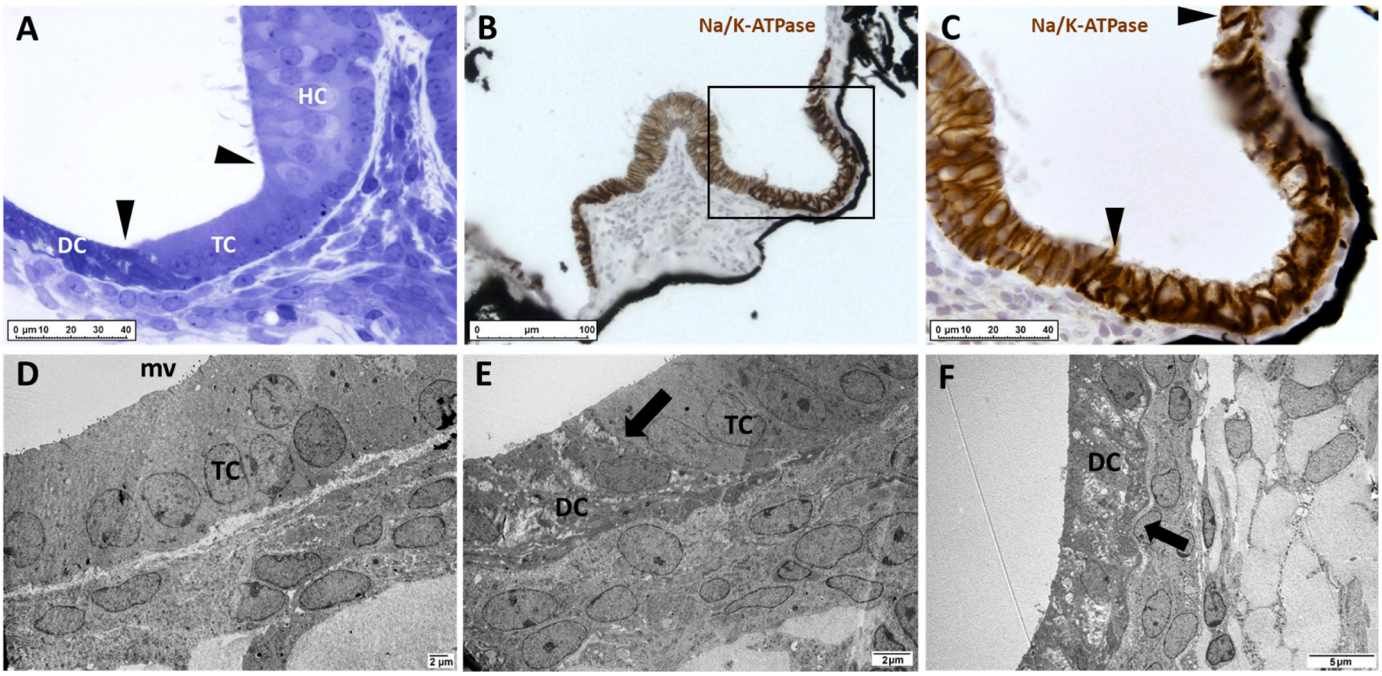

Fig. 4. Secretory area of 7-DIV cultured ampullae. (A) Light microscopy image of a transverse semi-thin section of secretory area of a 7-DIV 3D cultured ampullae obtained from P1 newborn rat. The black arrowheads delimit the transitional cell zone from the sensory epithelium and the dark cell zone. (B-C) Immuno-detection of Na/K-ATPase (brown) in 3D cultured ampullae (P3) observed by light microscopy at 7 DIV. Image (C) is a high magnification of the area delineated by the black square in (B). The black arrowheads delimit the dark cell area. (D-F) Ultrastructure of the secretory area of 3D ampullar explants (P1), as observed by transmission electron microscopy at 7 DIV. (D) Elongated transitional cells (TC) express microvilli (mv) at their apical side. (E) Secretory area is composed of cuboidal dark cells (DC) and transitional cells (TC). Black arrow indicates the delimitation between dark and transitional cells. (F) Ultrastructure of cuboidal dark cells. Black arrow indicates invaginations on the basal side.

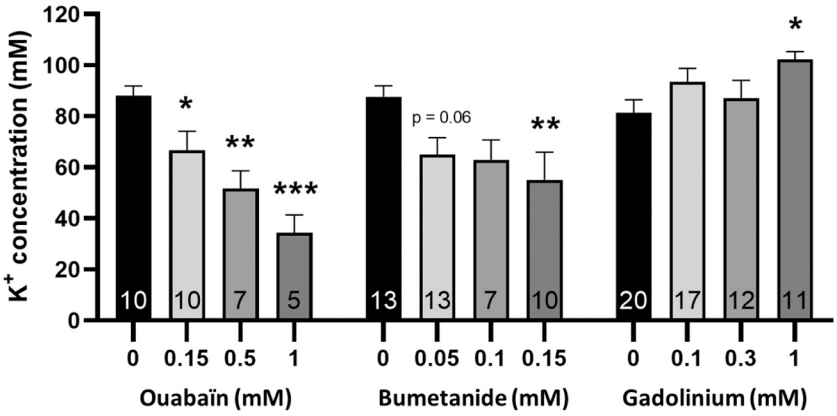

Fig. 5. Effects of inhibition of potassium ion pump and channels on endolymph K^+ concentration. 7-DIV cultured ampullae (P0-P4) were treated with gadolinium for 2 h, ouabain for 2 h or bumetanide for 30 min at three concentrations. Control samples were cultured in the same conditions with the corresponding vehicle. Each histogram represents the mean of repeated experiments ± SEM. The number of samples for each group is indicated at the bottom of the histogram. Asterisks indicate significant differences between control groups (black bar) and treated groups (gray bars). Dunnett: *$p < 0.05$, **$p < 0.01$ and ***$p < 0.001$.

intercalated supporting cells on the basal side. The secretory areas were composed of transitional and cuboidal dark cells, as shown in Fig. 4. No morphological defects or vacuoles were observed in epithelial cells, and nuclei had a normal aspect.

In cultures exposed for 2 h, normal epithelial cells were observed in both sensory epithelium and the secretory area, whatever the styrene concentration. Conversely, longer exposure times (72 h) induced histologically-observable dose-dependent damage. Thus, although no evidence of cellular stress was observed in samples exposed to 0.5 mM styrene for 72 h, exposure to 0.75 mM styrene led to the formation of cytoplasmic vacuoles in epithelial cells in both sensory and secretory areas. No other obvious features of cell alteration were present. Samples exposed to 1 mM styrene for 72 h displayed numerous pathological features including absence of cellular delimitation, and swollen and condensed nuclei. These observations suggest that styrene induces irreversible damage to epithelial cells in both secretory and sensory areas in our model.

ATP levels were quantified in 7-DIV cultured ampullae (P2-P4) exposed to 1 mM styrene for 2–72 h (Fig. 8). A time-dependent decrease in ATP level was observed [$F(6, 62) = 10.44$; $p < 0.001$]. The ATP concentration was significantly reduced from 6 h until the end of the exposure period. Between 6 h and 48 h, a relatively steady decline in ATP concentration was measured (6 h: 57%, $p < 0.001$; 24 h: 45%, $p = 0.004$; 48 h: 52%, $p < 0.001$). The greatest decrease (66%; $p < 0.001$) was reported after exposure for 72 h.

4. Discussion

The aim of this study was to develop a 3D cultured ampullae model that could be used to evaluate the vestibulotoxicity of aromatic

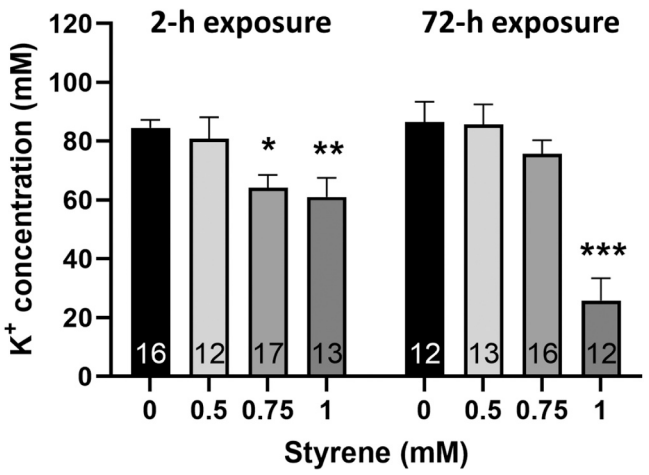

Fig. 6. Effects of styrene exposure on endolymph K^+ concentration. 7-DIV cultured ampullae were obtained from P0-P4 newborn rats and exposed to styrene (0.5, 0.75 or 1 mM) for 2 h or 72 h. Two-hour exposures were performed at 7 DIV and 72-h exposures between 4 and 7 DIV. Control samples were maintained in the same experimental conditions without styrene. Each histogram represents the mean of repeated experiments ± SEM. The number of samples for each group is indicated at the bottom of the histogram. Asterisks indicate significant differences between control groups (black bar) and treated groups (gray bars). Dunnett: *$p < 0.05$, **$p < 0.01$ and ***$p < 0.001$.

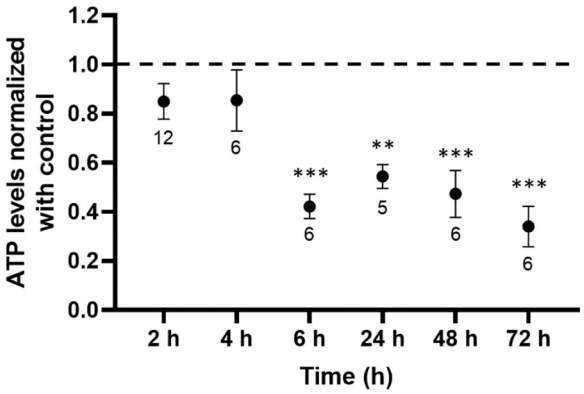

Fig. 8. 1-mM styrene exposure leads to decreased ATP levels over time. ATP was quantified by bioluminescence in ampullae derived from P2-P4 newborn rats and cultured for 7 DIV. Samples were exposed to 1 mM styrene for different durations (2 h; 4 h; 6 h; 24 h; 48 h or 72 h), and ATP was quantified at 7 DIV. Control samples were cultured in sealed vials without styrene. ATP levels measured in experimental groups were normalized relative to the mean control value (dotted line) obtained from all control samples (n = 38). Data for exposed groups represent mean ATP levels normalized relative to control, and error bars correspond to SEM. The number of samples for each exposed group is indicated below each symbol. Asterisks indicate significant differences between control and exposed data. Dunnett: **$p < 0.01$ and ***$p < 0.001$.

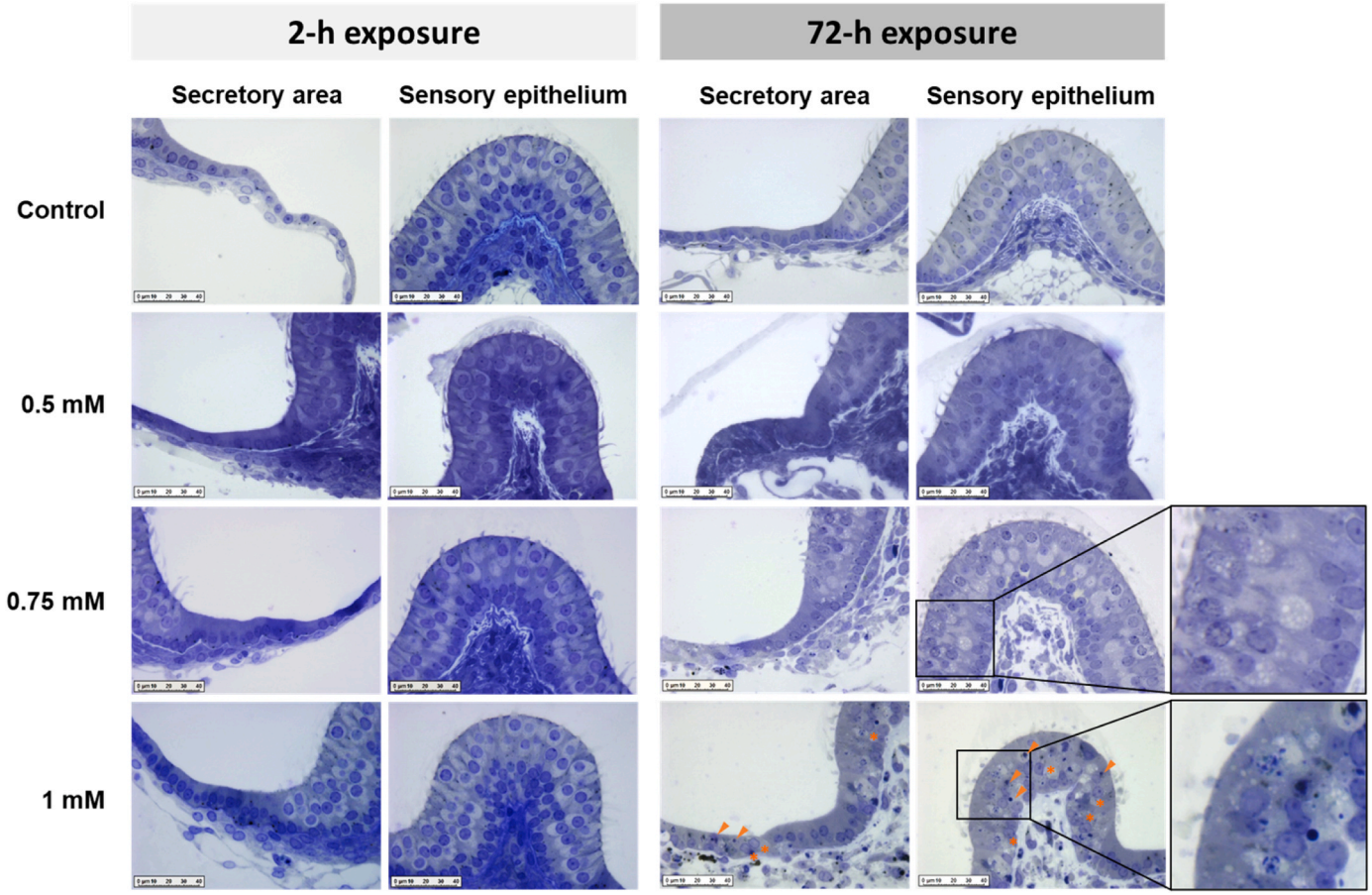

Fig. 7. Histological analysis of 7-DIV cultured ampullae exposed to styrene. Samples obtained from P0-P4 newborn rats were observed under light microscopy after exposure to styrene (0.5; 0.75 or 1 mM) for 2 or 72 h. Areas delineated by a black square were further magnified. Swollen nuclei are indicated by asterisks, and condensed nuclei by arrowheads. Scale bar = 40 μm.

compounds. The model was adapted from the method described by Bartolami et al. (2011) and Gaboyard et al. (2005), that we previously used to produce 3D cultured utricles (Tallandier et al., 2021, 2020).

In this paper, we present and characterize a cultured ampulla model that forms – *de novo* – a delimited compartment filled with an endolymph-like fluid. Although several studies have previously reported the use of short-lived 2D preparations of crista ampullaris to evaluate vestibulotoxicity (Dalian et al., 2012; Ding et al., 2018), no study described results obtained with long-term 3D cultures. To the best of our knowledge, this is the first report of successful culture of ampullar explants. After a few days in culture, electrophysiological and histological data confirmed that epithelial cells in the ampullae have a mature morphology and can maintain K^+ homeostasis. We used the model to assess the effects of, and infer the mechanisms behind, styrene toxicity in this region of the vestibular receptor.

4.1. Development of cultured ampullae

Morphological changes and K^+ concentrations monitored over time demonstrated that ampullae, like utricles (Tallandier et al., 2020), formed a closed compartment that gradually filled with a high-potassium fluid (Fig. 1). Thus, ampullae seeded in a gelatinous matrix sealed themselves on the first day of culture to form the endolymphatic compartment. BrdU staining at 2 DIV suggested that this first stage in explant development could involve canalar cell proliferation (Fig. 1**B**). Proliferation of these cells appears to promote reconstruction of the membranous wall to create a closed endolymphatic compartment. The mechanical properties of the Matrigel® matrix and the growth factors – such as EGF, *b*-FGF, and IGF-1 – present, as well as the N-2 supplement, could contribute to inducing epithelial cell proliferation in vestibular end-organs (Gnedeva et al., 2017; Zheng et al., 1997). In addition, in the first days of postnatal development, vestibular epithelial cells have a high proliferation capacity, as demonstrated by Gu et al. (2007). Indeed, these authors report the maximal proliferative response to growth factors of rat sensory epithelium to occur between P0 and P5. This timeline is in accordance with the age of the neonates used here.

The accumulation of K^+ ions in the endolymphatic compartment occurs in parallel to swelling of the cultured ampullae (Fig. 1A-D). These processes were similar to those observed with 3D cultured utricles from newborn rats (Tallandier et al., 2020). Once closed at 1 DIV, the ampullae displayed a vesicle which progressively swells until reaches its maximal size at 5 DIV. The K^+ accumulation, between 2 and 4 DIV, could cause water to enter in the endolymphatic compartment by osmosis and the structure to swell.

The endolymphatic K^+ concentration in ampullae at 7 DIV (85.3 $\pm$ 3.0 mM; Fig. 1D) was close to the concentrations measured in cultured utricles at the same DIV (85.8 $\pm$ 4.8 mM) (Tallandier et al., 2020). However, the K^+ concentrations measured here were slightly lower than *in vivo* values (107–144 mM: Citron and Exley, 1957; Dravis et al., 2007; Royaux et al., 2003; Smith et al., 1954). Similar discrepancies between *in vitro* and *in vivo* K^+ concentrations in the vestibular labyrinth have been reported for chicken embryo ampullae (Masetto et al., 2005). This difference could be explained by the lack of extracellular factors involved in K^+ secretion (*e.g.,* adrenergic hormones) in the 3D culture medium (Milhaud et al., 2002; Sunose et al., 1997; Wangemann et al., 1999).

The high K^+ concentration in endolymph results from K^+ secretion and absorption by vestibular epithelial cells (Ciuman, 2009). Morphological and physiological evidence indicates that all vestibular cells involved in K^+ cycling in the inner ear are preserved in the cultured explant (Figs. 2–5).

The curved sensory epithelium and the hair cells observed in 7-DIV 3D ampullar explants (Fig. 3C-E) had the same morphological aspects as *in vivo crista* surface preparations from a P7 rat (Dechesne et al., 1986; Wubbels et al., 2002). Two morphologically distinct hair-cell types were visible in our model at 7 DIV (Fig. 3F-H), and can be considered a feature of maturation of the vestibular sensory epithelium. Indeed, Meza et al. (1996) reported that hair cells could be characterized according to types I and II from the 4th postnatal day in rat *crista ampullaris*. Although hair-cell maturation continues after birth (Dechesne et al., 1986; Sans and Chat, 1982; Zheng and Gao, 1997), mouse hair-cell mechanotransduction is known to be acquired at embryonic stages (Géléoc and Holt, 2003), and basolateral conductance (g_{DR}) in type I and II hair cells develops over the first postnatal week (Hurley et al., 2006; Li et al., 2010; Meredith and Rennie, 2016). In addition to their role in mechanotransduction, hair cells play a key role in K^+ efflux. K^+ recycling begins with the uptake of potassium ions by hair cells *via* MET channels, followed by its secretion on the basolateral side into the perilymph thorough outwardly-rectifying K^+ channels (Meredith and Rennie, 2016; Pickles and Corey, 1992). Here, we assessed the K^+ efflux capacity of MET channels present on hair cells in ampullae using the well-known MET channel blocker, gadolinium (Kimitsuki et al., 1996) (Fig. 5). Gadolinium treatment effectively inhibited K^+ efflux mechanisms, indicating that MET channels present on hair cells actively participate in K^+ efflux in the model. In cultured ampullae, the increase in K^+ concentration following gadolinium treatment was only significant with the 1-mM concentration. In contrast, in our previous study using 3D cultured utricles, increased K^+ was observed with as little as 0.1 mM gadolinium (Tallandier et al., 2020). This discrepancy may be due to the fact that there are about 1.5-fold more hair cells in the macula of the utricule than in the crista (Desai et al., 2005b, 2005a). Here, the blockade of MET channels by 1 mM gadolinium led to a moderate (25%) increase in K^+ concentration after 2 h (Fig. 5). These findings, obtained with static 3D cultures, are in accordance with the small fraction (10–20%) of hair cells displaying the maximal level of MET conductance (g_{met}) when stereocilia are in an undisturbed position (Howard et al., 1988; Roberts et al., 1988). Moreover, the moderate K^+ increase observed after gadolinium treatment was not dose-dependent. This mild effect of gadolinium on K^+ concentrations may be due to modulation of K^+ secretion by dark cells, to regulate the ion composition of the endolymph (Marcus et al., 1994; Wangemann et al., 1996). In other words, the increase in K^+ concentration in the endolymphatic compartment induced by MET channel blockade following gadolinium treatment could lead to reduced potassium secretion in order to maintain a constant K^+ concentration in the endolymph. Whatever the case, our data provide morphological evidence of the presence of mature hair cells and demonstrate that MET channels present on hair cells in 3D cultured ampullae are functional.

The high K^+ concentration in the vestibular endolymph is maintained by secretory cells (Lang et al., 2007). Although the role of transitional cells in regulating ion levels in the endolymph and protecting hair cells against overstimulation has been extensively studied (Jeong et al., 2020; Lee et al., 2001; Nicolas et al., 2004; Popper et al., 2008; Takimoto et al., 2018), their potassium secretion activity is less well known. Transitional cells express NKCC1 and Na/K-ATPase at their basolateral pole (Pitovski and Kerr, 2002; Young Choi et al., 2005), and these cells are known to be involved in K^+ secretion at immature stages (Bartolami et al., 2011). For this reason, we assumed transitional cells to be secretory cells in our model. Histological observations confirmed that transitional cells bordered the sensory epithelium in 3D cultured ampullae (Fig. 2D, Fig. 3F and Fig. 4A, D-C), and their morphology was consistent with previous descriptions (Gaboyard et al., 2005; Igarashi, 1989).

In contrast, dark cells have long been known to be involved in K^+ secretion into the vestibular endolymph. These cells – with their cytoplasmic vacuoles, cuboidal shape, elevated expression of Na/K-ATPase, and basolateral infoldings – were clearly visible in our histological analysis (Fig. 4). Their characteristics indicate significant secretory activity (Masuda et al., 1995, 1994; Pitovski and Kerr, 2002). The morphological and physiological maturation of dark cells reported in previous studies (Anniko and Nordemar, 1980; Anniko and Wroblewski, 1981) appears to coincide with the changes to K^+ concentration over

time measured in our model (Fig. 1D). As previously demonstrated *in vivo*, the morphological maturation of dark cells could be linked to the rise of endolymphatic K^+ concentration (Anniko and Nordemar, 1980; Anniko and Wroblewski, 1981). Although the main K^+ secretion channels present in dark cells – Na/K-ATPase on the basolateral side and KCNQ1/E1 on the apical surface – are expressed from P1, the number of interdigitations toward the basolateral side increases between P1 and P4 (Anniko, 1980; Anniko and Nordemar, 1980; Nicolas et al., 2001; Peters et al., 2001). This timeline coincides with a 2-fold increase in the K^+ concentration in our model.

We studied K^+ secretion mechanisms using ouabain and bumetanide to inhibit Na/K-ATPase and NKCC1, respectively (Fig. 5). Treatment with bumetanide moderately decreased the K^+ concentration, but only the highest concentration (0.15 mM) had a statistically significant effect. These results are in accordance with those obtained by Marcus (1986), who reported a similar effect on K^+ secretion in isolated non-sensory regions with 0.01 mM or 0.1 mM bumetanide. However, *in vitro*, the same author reported a considerable reduction (94%) of K^+ secretion in the dark cell region at adulthood following treatment with 0.01 mM bumetanide (Marcus et al., 1994). The lower impact of bumetanide in our model could be explained by the lower level of NKCC1 expression in immature dark cells compared to adult cells, where NKCC1 is found on both dark and transitional cells (Bartolami et al., 2011; Young Choi et al., 2005).

A strong effect of ouabain on K^+ secretion has been extensively reported in adult dark and transitional cells (Marcus et al., 1994; Marcus and Shipley, 1994; Wangemann and Marcus, 1989). In our model, treatment with ouabain also led to a dose-dependent decrease in K^+ levels. Thus, our results demonstrated that Na/K-ATPase inhibition had a stronger impact on endolymphatic K^+ concentration than NKCC1 inhibition. This could be explained by the fact that inhibition of Na/K-ATPase may also affect NKCC1 activity. Indeed, the Na/K-ATPase pump moves 2 K^+ in and 3 Na^+ out (Schwartz et al., 1972), creating a Na^+ gradient that triggers NKCC1 function (Wangemann, 1995). Taken together, our electrophysiological results confirm that the two main K^+ influx mechanisms – involving Na/K-ATPase and NKCC1 – are functional in 3D cultured ampullae.

4.2. Effects of styrene exposure

Several studies have shown solvents to have a negative impact on vestibular function (Calabrese et al., 1996; Möller et al., 1990; Niklasson et al., 1993). In rat utricular explants exposed to such compounds, we previously demonstrated ionic and histological disruption (Tallandier et al., 2021, 2020). Here, we tested the hypothesis that the vestibulotoxic properties of styrene – one of the most widely-used aromatic solvents in industry – also included damage to ampulla.

Rats exposed to styrene show an auditory deficit associated with disruption of cochlear cells. Some experimental studies have provided evidence that outer hair cells (OHC) and supporting cells in the organ of Corti are both vulnerable to styrene (Campo et al., 1999; Chen et al., 2007; Chen and Henderson, 2009; Fetoni et al., 2021). As supporting cells surrounding the sensory epithelium play a determinant role in recycling potassium from the endolymph, it was hypothesized that styrene not only disrupts OHC, but that it also perturbs the ion balance in inner-ear fluids (Campo et al., 2001; Fetoni et al., 2016; Hibino and Kurachi, 2006; Spicer and Schulte, 1998). Both the vestibular end-organs and the cochlea contain endolymph. These two structures are composed of sensory hair cells, bearing crucial MET channels, and secretory cells – vestibular dark cells and cochlear marginal cells –which are involved in maintaining endolymphatic K^+ homeostasis (Lang et al., 2007; Wangemann, 1995). For these reasons, we chose to investigate the toxic mechanisms of styrene based on both histological observations of sensory and secretory epithelium, and by measuring the endolymphatic K^+ concentration.

The durations of styrene exposure (2–72 h) were initially chosen to discriminate between acute and cytotoxic effects. Indeed, some aromatic solvents could acutely affect the activity of ion channels, such as voltage-dependent Ca^{2+} channels, Na/K-ATPase, or N-methyl-D-aspartate (NMDA) and nicotinic receptors (Bale et al., 2005; Cruz et al., 2000; Shafer et al., 2005; Vaalavirta and Tähti, 1995). Cytotoxic effects of styrene have been reported with *in vitro* models in conditions comparable (concentration and duration exposure) to those used here (Diodovich et al., 2004; Kohn et al., 1995). To avoid any interaction between the styrene effect and the development of 3D cultured explants, the 72-h exposure was performed from 4 to 7 DIV, after the K^+ level had plateaued (Fig. 1D).

Our results showed that styrene caused a moderate K^+ concentration decrease starting at 0.75 mM after a 2-h exposure, and a steep decline at 1 mM after exposure for 72 h (Fig. 6). In cultured utricles from newborn rats, we had previously demonstrated a significant decrease in K^+ concentration after exposure to 0.75 mM styrene for 2 h (Tallandier et al., 2020). Despite a significant decrease in K^+ concentration after exposure to 0.75 mM and 1 mM styrene for 2 h, 3D ampulla cultures displayed no histopathological features. Conversely, samples exposed to 1 mM styrene for 72 h displayed numerous pathological features indicative of irreversible lesions – absence of cellular delimitation, swollen and condensed nuclei – in both secretory and sensory epithelium, along with a strong decrease in K^+ concentration (Figs. 6 and 7).

Even though cytoplasmic vacuoles were observed after exposure to 0.75 mM styrene for 72 h, the decrease in K^+ level was not significant. In some cases, vacuoles may be transient, and they are not always associated with cell death. Vacuole formation may be an initiating event induced by a cytotoxic compound causing stress responses that can lead to irreversible damage in worst case (Shubin et al., 2016). Although the mechanisms remain unclear, cytoplasmic vacuoles could be an adaptative response to cellular stress, and may be linked to endocytosis (Debnath et al., 2005; Wang and Klionsky, 2003). Thus, the effect of 0.75 mM styrene observed after exposure for 72 h may be reversible. Additional work will be necessary to decipher the mechanisms induced by styrene exposure in our model.

Cultured ampullae exposed to 1 mM styrene displayed a significant decline of ATP levels after 6 h (**Fig. 8**). It is well established that intracellular ATP levels determine cell death fate by apoptosis or necrosis. Apoptotic cell death requires energy, whereas a rapid drop in ATP levels triggers necrosis (Eguchi et al., 1997; Leist et al., 1997; Leist and Nicotera, 1997; Tsujimoto, 1997). The rapid reduction of ATP level and the characteristic histopathological features – swollen nuclei and membrane disruption – observed after styrene exposure (Figs. 7 and 8) suggest that styrene induces necrotic rather than apoptotic mechanisms in our model. These results are in accordance with our previous study, where we demonstrated that styrene does not induce cell death by apoptosis in cultured utricles (Tallandier et al., 2020).

The reduced K^+ concentration measured after 72-h exposure to 1 mM styrene could be the consequence of its cytotoxic effects. Indeed, energy depletion causes ion pumps to fail, resulting in disrupted ion and water fluxes. These effects could subsequently lead to irreversible histological damage, such as nuclear swelling or membrane disruption. Events of this type have already been described following a lethal injury such as stroke or chemical toxicity (Loh et al., 2019; Majno and Joris, 1995; Trump et al., 1997; Van Cruchten and Van Den Broeck, 2002; Weerasinghe and Buja, 2012). However, the decrease in K^+ concentration measured in cultures exposed to styrene for 2 h was not associated with reduced ATP levels or histopathological effects (Figs. 6, 7, and 8). Therefore, we cannot consider that the effect on K^+ concentration was due to decreased ATP levels or to cellular disruption. Styrene might disrupt membrane fluidity or exert a pharmacological action that could impair the activity of ion channels and transporters (Franks and Lieb, 2004, 1984; Rauchová et al., 1999; Tanii et al., 1994). Either of these mechanisms could explain the acute effects of styrene on K^+ concentration observed here, but additional studies will be necessary to verify these hypotheses.

Although the acute effect of styrene on K^+ concentration was similar with 0.75 mM and 1 mM, the drop in K^+ concentration was amplified after 72 h only with 1 mM styrene. This finding suggests that exposure to lower doses of styrene (0.75 mM) for 72 h was not sufficient to trigger an irreversible cytotoxic effect in our model.

5. Conclusion

To improve our understanding of the effects of toxic compounds on vestibular end-organs, we developed a 3D cultured ampulla model. Although cultured utricular explants have been used to study the effects of aromatic solvents on the vestibular receptor, ampullae are of interest as they make toxicological investigations more ethical (6 samples per animal) and provide information on their effect on a different vestibular epithelium. This new model recreates an endolymphatic compartment *de novo*, that fills with a high-potassium (K^+) endolymph-like fluid, by the same mechanisms as those described *in vivo* (K^+ influx by secretory cells and K^+ efflux by hair cells). Although *in vivo* studies are required to validate any findings, cultured ampullae can be used to gain insights into a range of mechanisms (acute and cytotoxic effects) involved in the vestibulotoxicity of industrial compounds.

Funding

This research did not receive any specific grant from funding agencies in the public, commercial, or not-for-profit sectors.

CRediT authorship contribution statement

V.T. conceptualized and designed experiments. V.T. and L.M. performed 3D cultures, electrophysiological recordings, aromatic solvent exposure experiments, and pharmacological treatments. V.T. performed ATP assays. V.T. and T.V. were responsible for data acquisition and analyses. A.T. and S.B. prepared histological samples, and acquired images. V.T. drafted the manuscript. B.P. and M.C. supervised the investigation and revised the manuscript. All authors have read and approved the published version of the manuscript.

Declaration of Competing Interest

The authors declare that they have no known competing financial interests or personal relationships that could have appeared to influence the work reported in this paper.

Data Availability

Data will be made available on request.

References

Anniko, M., 1980. Embryologic development in vivo and in vitro of the dark cell region of the mammalian crista ampullaris. Acta Otolaryngol. 90, 106–114. https://doi.org/10.3109/00016488009131705.

Anniko, M., Nordemar, H., 1980. Embryogenesis of the inner ear. IV. Post-natal maturation of the secretory epithelia of the inner ear in correlation with the elemental composition in the endolymphatic space. Arch. Otorhinolaryngol. 229, 281–288. https://doi.org/10.1007/BF02565531.

Anniko, M., Wroblewski, R., 1981. Elemental composition of the developing inner ear. Ann. Otol., Rhinol., Laryngol. 90, 25–32. https://doi.org/10.1177/000348948109000107.

Bale, A.S., Meacham, C.A., Benignus, V.A., Bushnell, P.J., Shafer, T.J., 2005. Volatile organic compounds inhibit human and rat neuronal nicotinic acetylcholine receptors expressed in Xenopus oocytes. Toxicol. Appl. Pharmacol. 205, 77–88. https://doi.org/10.1016/j.taap.2004.09.011.

Bartolami, S., Gaboyard, S., Quentin, J., Travo, C., Cavalier, M., Barhanin, J., Chabbert, C., 2011. Critical roles of transitional cells and Na/K-ATPase in the formation of vestibular endolymph. J. Neurosci. 31, 16541–16549. https://doi.org/10.1523/JNEUROSCI.2430-11.2011.

Calabrese, G., Martini, A., Sessa, G., Cellini, M., Bartolucci, G.B., Marcuzzo, G., De Rosa, E., 1996. Otoneurological study in workers exposed to styrene in the fiberglass industry. Int. Arch. Occup. Environ. Health 68, 219–223. https://doi.org/10.1007/BF00381431.

Campo, P., Lataye, R., Loquet, G., Bonnet, P., 2001. Styrene-induced hearing loss: a membrane insult. Hear. Res. 154, 170–180. https://doi.org/10.1016/s0378-5955(01)00218-0.

Campo, P., Loquet, G., Blachère, V., Roure, M., 1999. Toluene and styrene intoxication route in the rat cochlea. Neurotoxicol. Teratol. 21, 427–434. https://doi.org/10.1016/s0892-0362(99)00010-0.

Chen, G.-D., Chi, L.-H., Kostyniak, P.J., Henderson, D., 2007. Styrene induced alterations in biomarkers of exposure and effects in the cochlea: mechanisms of hearing loss. Toxicol. Sci. 98, 167–177. https://doi.org/10.1093/toxsci/kfm078.

Chen, G.-D., Henderson, D., 2009. Cochlear injuries induced by the combined exposure to noise and styrene. Hear. Res. 254, 25–33. https://doi.org/10.1016/j.heares.2009.04.005.

Citron, L., Exley, D., 1957. Recent work on the biochemistry of the labyrinthine fluids. Proc. R. Soc. Med 50, 697–701.

Ciuman, R.R., 2009. Stria vascularis and vestibular dark cells: characterisation of main structures responsible for inner-ear homeostasis, and their pathophysiological relations. J. Laryngol. Otol. 123, 151. https://doi.org/10.1017/S0022215108002624.

Cruz, S.L., Balster, R.L., Woodward, J.J., 2000. Effects of volatile solvents on recombinant N-methyl-D-aspartate receptors expressed in Xenopus oocytes. Br. J. Pharm. 131, 1303–1308. https://doi.org/10.1038/sj.bjp.0703666.

Dalian, D., Haiyan, J., Yong, F., Salvi, R., Someya, S., Tanokura, M., 2012. Ototoxic effects of carboplatin in organotypic cultures in chinchillas and rats. J. Otol. 7, 92–102. https://doi.org/10.1016/S1672-2930(12)50023-1.

Debnath, J., Baehrecke, E.H., Kroemer, G., 2005. Does autophagy contribute to cell death? Autophagy 1, 66–74. https://doi.org/10.4161/auto.1.2.1738.

Dechesne, C., Mbiene, J.P., Sans, A., 1986. Postnatal development of vestibular receptor surfaces in the rat. Acta Otolaryngol. 101, 11–18. https://doi.org/10.3109/00016488609108602.

Desai, S.S., Ali, H., Lysakowski, A., 2005a. Comparative morphology of rodent vestibular periphery. II. Cristae ampullares. J. Neurophysiol. 93, 267–280. https://doi.org/10.1152/jn.00747.2003.

Desai, S.S., Zeh, C., Lysakowski, A., 2005b. Comparative morphology of rodent vestibular periphery. I. Saccular and utricular maculae. J. Neurophysiol. 93, 251–266. https://doi.org/10.1152/jn.00746.2003.

Ding, D., Jiang, H., Zhang, J., Xu, X., Qi, W., Shi, H., Yin, S., Salvi, R., 2018. Cisplatin-induced vestibular hair cell lesion-less damage at high doses. J. Otol. 13, 115–121. https://doi.org/10.1016/j.joto.2018.08.002.

Diodovich, C., Bianchi, M.G., Bowe, G., Acquati, F., Taramelli, R., Parent-Massin, D., Gribaldo, L., 2004. Response of human cord blood cells to styrene exposure: evaluation of its effects on apoptosis and gene expression by genomic technology. Toxicology 200, 145–157. https://doi.org/10.1016/j.tox.2004.03.021.

Dravis, C., Wu, T., Chumley, M.J., Yokoyama, N., Wei, S., Wu, D.K., Marcus, D.C., Henkemeyer, M., 2007. EphB2 and ephrin-B2 regulate the ionic homeostasis of vestibular endolymph. Hear. Res. 223, 93–104. https://doi.org/10.1016/j.heares.2006.10.007.

Eguchi, Y., Shimizu, S., Tsujimoto, Y., 1997. Intracellular ATP levels determine cell death fate by apoptosis or necrosis. Cancer Res. 57, 1835–1840.

Fetoni, A.R., Paciello, F., Rolesi, R., Pisani, A., Moleti, A., Sisto, R., Troiani, D., Paludetti, G., Grassi, C., 2021. Styrene targets sensory and neural cochlear function through the crossroad between oxidative stress and inflammation. Free Radic. Biol. Med. 163, 31–42. https://doi.org/10.1016/j.freeradbiomed.2020.12.001.

Fetoni, A.R., Rolesi, R., Paciello, F., Eramo, S.L.M., Grassi, C., Troiani, D., Paludetti, G., 2016. Styrene enhances the noise induced oxidative stress in the cochlea and affects differently mechanosensory and supporting cells. Free Radic. Biol. Med. 101, 211–225. https://doi.org/10.1016/j.freeradbiomed.2016.10.014.

Franks, N.P., Lieb, W.R., 2004. Seeing the light: protein theories of general anesthesia. Anesthesiolology 101, 235–237. https://doi.org/10.1097/00000542-200407000-00034.

Franks, N.P., Lieb, W.R., 1984. Do general anaesthetics act by competitive binding to specific receptors. Nature 310, 599–601. https://doi.org/10.1038/310599a0.

Gaboyard, S., Chabbert, C., Travo, C., Bancel, F., Lehouelleur, J., Yamauchi, D., Marcus, D.C., Sans, A., 2005. Three-dimensional culture of newborn rat utricle using an extracellular matrix promotes formation of a cyst. Neuroscience 133, 253–265. https://doi.org/10.1016/j.neuroscience.2005.02.011.

Gagnaire, F., Langlais, C., 2005. Relative ototoxicity of 21 aromatic solvents. Arch. Toxicol. 79, 346–354. https://doi.org/10.1007/s00204-004-0636-2.

Gans, R.E., Rauterkus, G., Research Associate 1, 2019. Vestibular toxicity: causes, evaluation protocols, intervention, and management. Semin Hear 40, 144–153. https://doi.org/10.1055/s-0039-1684043.

Géléoc, G.S.G., Holt, J.R., 2003. Developmental acquisition of sensory transduction in hair cells of the mouse inner ear. Nat. Neurosci. 6, 1019–1020. https://doi.org/10.1038/nn1120.

Gnedeva, K., Jacobo, A., Salvi, J.D., Petelski, A.A., Hudspeth, A.J., 2017. Elastic force restricts growth of the murine utricle. Elife 6. https://doi.org/10.7554/eLife.25681.

Gu, R., Montcouquiol, M., Marchionni, M., Corwin, J.T., 2007. Proliferative responses to growth factors decline rapidly during postnatal maturation of mammalian hair cell epithelia. Eur. J. Neurosci. 25, 1363–1372. https://doi.org/10.1111/j.1460-9568.2007.05414.x.

Hibino, H., Kurachi, Y., 2006. Molecular and physiological bases of the K^+ circulation in the mammalian inner ear. Physiology 21, 336–345. https://doi.org/10.1152/physiol.00023.2006.

Howard, J., Roberts, W.M., Hudspeth, A.J., 1988. Mechanoelectrical transduction by hair cells. Annu Rev. Biophys. Biophys. Chem. 17, 99–124. https://doi.org/10.1146/annurev.bb.17.060188.000531.

Hurley, K.M., Gaboyard, S., Zhong, M., Price, S.D., Wooltorton, J.R.A., Lysakowski, A., Eatock, R.A., 2006. M-like K+ currents in type I hair cells and calyx afferent endings of the developing rat utricle. J. Neurosci. 26, 10253–10269. https://doi.org/10.1523/JNEUROSCI.2596-06.2006.

Igarashi, Y., 1989. Submicroscopic study of the vestibular dark cell area in human fetuses. Acta Oto-Laryngol. 107, 29–38. https://doi.org/10.3109/00016488909127476.

Jeong, J., Kim, J.Y., Hong, H., Wangemann, P., Marcus, D.C., Jung, J., Choi, J.Y., Kim, S. H., 2020. P2RX2 and P2RX4 receptors mediate cation absorption in transitional cells and supporting cells of the utricular macula. Hear. Res. 386, 107860 https://doi.org/10.1016/j.heares.2019.107860.

Johnson, A.-C., 2007. Relationship between styrene exposure and hearing loss: review of human studies. Int. J. Occup. Med. Environ. Health 20, 315–325. https://doi.org/10.2478/v10001-007-0040-2.

Kimitsuki, T., Nakagawa, T., Hisashi, K., Komune, S., Komiyama, S., 1996. Gadolinium blocks mechano-electric transducer current in chick cochlear hair cells. Hear. Res. 101, 75–80. https://doi.org/10.1016/S0378-5955(96)00134-7.

Kohn, J., Minotti, S., Durham, H., 1995. Assessment of the neurotoxicity of styrene, styrene oxide, and styrene glycol in primary cultures of motor and sensory neurons. Toxicol. Lett. 75, 29–37. https://doi.org/10.1016/0378-4274(94)03153-x.

Lang, F., Vallon, V., Knipper, M., Wangemann, P., 2007. Functional significance of channels and transporters expressed in the inner ear and kidney. Am. J. Physiol. -Cell Physiol. 293, C1187–C1208. https://doi.org/10.1152/ajpcell.00024.2007.

Larsby, B., Tham, R., Odkvist, L.M., Hydén, D., Bunnfors, I., Aschan, G., 1978. Exposure of rabbits to styrene. Electronystagmographic findings correlated to the styrene level in blood and cerebrospinal fluid. Scand. J. Work Environ. Health 4, 60–65. https://doi.org/10.5271/sjweh.2722.

Lee, J.H., Chiba, T., Marcus, D.C., 2001. P2×2 receptor mediates stimulation of parasensory cation absorption by cochlear outer sulcus cells and vestibular transitional cells. J. Neurosci. 21, 9168–9174. https://doi.org/10.1523/JNEUROSCI.21-23-09168.2001.

Leist, M., Nicotera, P., 1997. The shape of cell death. Biochem. Biophys. Res. Commun. 236, 1–9. https://doi.org/10.1006/bbrc.1997.6890.

Leist, M., Single, B., Castoldi, A.F., Kühnle, S., Nicotera, P., 1997. Intracellular adenosine triphosphate (ATP) concentration: a switch in the decision between apoptosis and necrosis. J. Exp. Med. 185, 1481–1486. https://doi.org/10.1084/jem.185.8.1481.

Li, G.Q., Meredith, F.L., Rennie, K.J., 2010. Development of K(+) and Na(+) conductances in rodent postnatal semicircular canal type I hair cells. Am. J. Physiol. Regul. Integr. Comp. Physiol. 298, R351–R358. https://doi.org/10.1152/ajpregu.00460.2009.

Loh, K.Y., Wang, Z., Liao, P., 2019. Oncotic Cell Death in Stroke. Rev. Physiol. Biochem. Pharm. 176, 37–64. https://doi.org/10.1007/112_2018_13.

Majno, G., Joris, I., 1995. Apoptosis, oncosis, and necrosis. An overview of cell death. Am. J. Pathol. 146, 3–15.

Marcus, D.C., 1986. Transepithelial electrical potential of nonsensory region of gerbil utricle in vitro. Am. J. Physiol. 251, C662–C670. https://doi.org/10.1152/ajpcell.1986.251.5.C662.

Marcus, D.C., Liu, J., Wangemann, P., 1994. Transepithelial voltage and resistance of vestibular dark cell epithelium from the gerbil ampulla. Hear. Res. 73, 101–108. https://doi.org/10.1016/0378-5955(94)90287-9.

Marcus, D.C., Shipley, A.M., 1994. Potassium secretion by vestibular dark cell epithelium demonstrated by vibrating probe. Biophys. J. 66, 1939–1942. https://doi.org/10.1016/S0006-3495(94)80987-7.

Masetto, S., Zucca, G., Bottà, L., Valli, P., 2005. Endolymphatic potassium of the chicken vestibule during embryonic development. Int. J. Dev. Neurosci. 23, 439–448. https://doi.org/10.1016/j.ijdevneu.2005.05.002.

Masuda, M., Yamazaki, K., Kanzaki, J., Hosoda, Y., 1995. Ultrastructural evidence of cell communication between epithelial dark cells and melanocytes in vestibular organs of the human inner ear. Anat. Rec. 242, 267–277. https://doi.org/10.1002/ar.1092420217.

Masuda, M., Yamazaki, K., Kanzaki, J., Hosoda, Y., 1994. Ultrastructure of melanocytes in the dark cell area of human vestibular organs: Functional implications of gap junctions, isolated cilia, and annulate lamellae. Anat. Rec. 240, 481–491. https://doi.org/10.1002/ar.1092400406.

Meredith, F.L., Rennie, K.J., 2016. Channeling your inner ear potassium: K(+) channels in vestibular hair cells. Hear. Res. 338, 40–51. https://doi.org/10.1016/j.heares.2016.01.015.

Meza, G., Acuña, D., Gutiérrez, A., Merchan, J.M., Rueda, J., 1996. Development of vestibular function: biochemical, morphological and electronystagmographical assessment in the rat. Int J. Dev. Neurosci. 14, 507–513. https://doi.org/10.1016/0736-5748(95)00099-2.

Milhaud, P.G., Pondugula, S.R., Lee, J.H., Herzog, M., Lehouelleur, J., Wangemann, P., Sans, A., Marcus, D.C., 2002. Chloride secretion by semicircular canal duct epithelium is stimulated via beta 2-adrenergic receptors. Am. J. Physiol., Cell Physiol. 283, C1752–C1760. https://doi.org/10.1152/ajpcell.00283.2002.

Möller, C., Odkvist, L., Larsby, B., Tham, R., Ledin, T., Bergholtz, L., 1990. Otoneurological findings in workers exposed to styrene. Scand. J. Work Environ. Health 16, 189–194. https://doi.org/10.5271/sjweh.1795.

Nicolas, M., Demêmes, D., Martin, A., Kupershmidt, S., Barhanin, J., 2001. KCNQ1/KCNE1 potassium channels in mammalian vestibular dark cells. Hear. Res. 153, 132–145. https://doi.org/10.1016/s0378-5955(00)00268-9.

Nicolas, M.-T., Lesage, F., Reyes, R., Barhanin, J., Demêmes, D., 2004. Localization of TREK-1, a two-pore-domain K+ channel in the peripheral vestibular system of mouse and rat. Brain Res 1017, 46–52. https://doi.org/10.1016/j.brainres.2004.05.012.

Nies, E., 2012. Ototoxic substances at the workplace: a brief update. Arh. Hig. Rada Toksikol. 63, 147–152. https://doi.org/10.2478/10004-1254-63-2012-2199.

Niklasson, M., Tham, R., Larsby, B., Eriksson, B., 1993. Effects of toluene, styrene, trichloroethylene, and trichloroethane on the vestibulo-and opto-oculo motor system in rats. Neurotoxicol Teratol. 15, 327–334. https://doi.org/10.1016/0892-0362(93)90034-l.

Odkvist, L.M., Larsby, B., Tham, R., Ahlfeldt, H., Andersson, B., Eriksson, B., Liedgren, S. R., 1982. Vestibulo-oculomotor disturbances in humans exposed to styrene. Acta Otolaryngol. 94, 487–493. https://doi.org/10.3109/00016488209128939.

Peters, T.A., Kuijpers, W., Curfs, J.H., 2001. Occurrence of NaK-ATPase isoforms during rat inner ear development and functional implications. Eur. Arch. Oto-Rhino-Laryngol.: Off. J. Eur. Fed. Oto-Rhino-Laryngol. Soc. (EUFOS): Affil. Ger. Soc. Oto-Rhino-Laryngol. - Head. Neck Surg. 258, 67–73. https://doi.org/10.1007/s004050000304.

Pickles, J.O., Corey, D.P., 1992. Mechanoelectrical transduction by hair cells. Trends Neurosci. 15, 254–259. https://doi.org/10.1016/0166-2236(92)90066-H.

Pitovski, D.Z., Kerr, T.P., 2002. Sodium- and potassium-activated ATPase in the mammalian vestibular system. Hear. Res. 171, 51–65. https://doi.org/10.1016/s0378-5955(02)00352-0.

Popper, P., Winkler, J., Erbe, C.B., Lerch-Gaggl, A., Siebeneich, W., Wackym, P.A., 2008. Distribution of two-pore-domain potassium channels in the adult rat vestibular periphery. Hear. Res. 246, 1–8. https://doi.org/10.1016/j.heares.2008.09.004.

Rauchová, H., Drahota, Z., Koudelová, J., 1999. The role of membrane fluidity changes and thiobarbituric acid-reactive substances production in the inhibition of cerebral cortex Na+/K+-ATPase activity. Physiol. Res 48, 73–78.

Roberts, W.M., Howard, J., Hudspeth, A.J., 1988. Hair cells: transduction, tuning, and transmission in the inner ear. Annu. Rev. Cell Biol. 4, 63–92. https://doi.org/10.1146/annurev.cb.04.110188.000431.

Royaux, I.E., Belyantseva, I.A., Wu, T., Kachar, B., Everett, L.A., Marcus, D.C., Green, E. D., 2003. Localization and Functional Studies of Pendrin in the Mouse Inner Ear Provide Insight About the Etiology of Deafness in Pendred Syndrome. JARO - J. Assoc. Res. Otolaryngol. 4, 394–404. https://doi.org/10.1007/s10162-002-3052-4.

Sans, A., Chat, M., 1982. Analysis of temporal and spatial patterns of rat vestibular hair cell differentiation by tritiated thymidine radioautography. J. Comp. Neurol. 206, 1–8. https://doi.org/10.1002/cne.902060102.

Schwartz, A., Lindenmayer, G.E., Allen, J.C., 1972. The Na+, K+-ATPase Membrane Transport System: Importance in Cellular Function. In: Current Topics in Membranes and Transport. Elsevier, pp. 1–82. https://doi.org/10.1016/S0070-2161(08)61057-6.

Shafer, T.J., Bushnell, P.J., Benignus, V.A., Woodward, J.J., 2005. Perturbation of Voltage-Sensitive Ca $^{2+}$ Channel Function by Volatile Organic Solvents. J. Pharm. Exp. Ther. 315, 1109–1118. https://doi.org/10.1124/jpet.105.090027.

Shubin, A.V., Demidyuk, I.V., Komissarov, A.A., Rafieva, L.M., Kostrov, S.V., 2016. Cytoplasmic vacuolization in cell death and survival. Oncotarget 7, 55863–55889. https://doi.org/10.18632/oncotarget.10150.

Sliwinska-Kowalska, M., Fuente, A., Zamyslowska-Szmytke, E., 2020. Cochlear dysfunction is associated with styrene exposure in humans. PLoS One 15, e0227978. https://doi.org/10.1371/journal.pone.0227978.

Smith, C.A., Lowry, O.H., Wu, M.L., 1954. The electrolytes of the labyrinthine fluids. Laryngoscope 64, 141–153. https://doi.org/10.1288/00005537-195403000-00001.

Spicer, S.S., Schulte, B.A., 1998. Evidence for a medial K+ recycling pathway from inner hair cells. Hear. Res. 118, 1–12. https://doi.org/10.1016/s0378-5955(98)00006-9.

Steyger, P.S., 2021. Mechanisms of Aminoglycoside- and Cisplatin-Induced Ototoxicity. Am. J. Audio 30, 887–900. https://doi.org/10.1044/2021_AJA-21-00006.

Sunose, H., Liu, J., Shen, Z., Marcus, D.C., 1997. cAMP increases apical IsK channel current and K+ secretion in vestibular dark cells. J. Membr. Biol. 156, 25–35. https://doi.org/10.1007/s002329900184.

Takimoto, Y., Ishida, Y., Kondo, M., Imai, T., Hanada, Y., Ozono, Y., Kamakura, T., Inohara, H., Shimada, S., 2018. P2×2 Receptor Deficiency in Mouse Vestibular End Organs Attenuates Vestibular Function. Neuroscience 386, 41–50. https://doi.org/10.1016/j.neuroscience.2018.06.026.

Tallandier, V., Chalansonnet, M., Merlen, L., Boucard, S., Thomas, A., Campo, P., Pouyatos, B., 2021. An in vitro model to assess the peripheral vestibulotoxicity of aromatic solvents. S0161813×21000255 NeuroToxicology. https://doi.org/10.1016/j.neuro.2021.03.002.

Tallandier, V., Merlen, L., Boucard, S., Thomas, A., Venet, T., Chalansonnet, M., Gauchard, G., Campo, P., Pouyatos, B., 2020. Styrene alters potassium endolymphatic concentration in a model of cultured utricle explants. Toxicol. Vitr., 104915 https://doi.org/10.1016/j.tiv.2020.104915.

Tanii, H., Huang, J., Ohyashiki, T., Hashimoto, K., 1994. Physical-chemical-activity relationship of organic solvents: effects on Na(+)-K(+)-ATPase activity and membrane fluidity in mouse synaptosomes. Neurotoxicol Teratol. 16, 575–582. https://doi.org/10.1016/0892-0362(94)90035-3.

Tham, R., Larsby, B., Eriksson, B., Bunnfors, I., Odkvist, L., Liedgren, C., 1982. Electronystagmographic findings in rats exposed to styrene or toluene. Acta Otolaryngol. 93, 107–112. https://doi.org/10.3109/00016488209130859.

Trump, B.F., Berezesky, I.K., Chang, S.H., Phelps, P.C., 1997. The pathways of cell death: oncosis, apoptosis, and necrosis. Toxicol. Pathol. 25, 82–88. https://doi.org/10.1177/019262339702500116.

Tsujimoto, Y., 1997. Apoptosis and necrosis: Intracellular ATP level as a determinant for cell death modes. Cell Death Differ. 4, 429–434. https://doi.org/10.1038/sj.cdd.4400262.

Vaalavirta, L., Tähti, H., 1995. Astrocyte membrane Na+, K(+)-ATPase and Mg(2+)-ATPase as targets of organic solvent impact. Life Sci. 57, 2223–2230. https://doi.org/10.1016/0024-3205(95)02214-4.

Van Cruchten, S., Van Den Broeck, W., 2002. Morphological and biochemical aspects of apoptosis, oncosis and necrosis. Anat. Histol. Embryol. 31, 214–223. https://doi.org/10.1046/j.1439-0264.2002.00398.x.

Wang, C.-W., Klionsky, D.J., 2003. The Molecular Mechanism of Autophagy. Mol. Med 9, 65–76. https://doi.org/10.1007/BF03402040.

Wangemann, P., 1995. Comparison of ion transport mechanisms between vestibular dark cells and strial marginal cells. Hear. Res. 90, 149–157. https://doi.org/10.1016/0378-5955(95)00157-2.

Wangemann, P., Liu, J., Shimozono, M., Scofield, M.A., 1999. Beta1-adrenergic receptors but not beta2-adrenergic or vasopressin receptors regulate K+ secretion in vestibular dark cells of the inner ear. J. Membr. Biol. 170, 67–77. https://doi.org/10.1007/s002329900538.

Wangemann, P., Marcus, D.C., 1989. Membrane potential measurements of transitional cells from the crista ampullaris of the gerbil. Effects of barium, quinidine, quinine, tetraethylammonium, cesium, ammonium, thallium and ouabain. Pflug. Arch. 414, 656–662. https://doi.org/10.1007/BF00582132.

Wangemann, P., Shen, Z., Liu, J., 1996. K(+)-induced stimulation of K+ secretion involves activation of the IsK channel in vestibular dark cells. Hear. Res. 100, 201–210. https://doi.org/10.1016/0378-5955(96)00127-x.

Weerasinghe, P., Buja, L.M., 2012. Oncosis: an important non-apoptotic mode of cell death. Exp. Mol. Pathol. 93, 302–308. https://doi.org/10.1016/j.yexmp.2012.09.018.

Wubbels, R.J., de Jong, H. a A., van Marle, J., 2002. Morphometric analysis of the vestibular sensory epithelia of young adult rat. J. Vesti Res 12, 145–154.

Young Choi, J., Ho Jung, S., Namkung, W., Lee, J.-H., Jin Son, E., Wook Shin, J., Park, H. Y., Sang Lee, W., Kim, H.N., 2005. Vestibular malformation in mice lacking Na-K-2Cl cotransporter 1 and expression of Na-K-2Cl cotransporter 1 in human vestibular end organs. Acta Otolaryngol. 125, 1252–1257. https://doi.org/10.1080/00016480510012309.

Zamyslowska-Szmytke, E., Sliwinska-Kowalska, M., 2011. Vestibular and balance findings in nonsymptomatic workers exposed to styrene and dichloromethane. Int J. Audio 50, 815–822. https://doi.org/10.3109/14992027.2011.599872.

Zheng, J.L., Gao, W.Q., 1997. Analysis of rat vestibular hair cell development and regeneration using calretinin as an early marker. J. Neurosci. 17, 8270–8282. https://doi.org/10.1523/JNEUROSCI.17-21-08270.1997.

Zheng, J.L., Helbig, C., Gao, W.Q., 1997. Induction of cell proliferation by fibroblast and insulin-like growth factors in pure rat inner ear epithelial cell cultures. J. Neurosci. 17, 216–226. https://doi.org/10.1523/JNEUROSCI.17-01-00216.1997.